Bars in early- and late-type discs in COSMOS

E. Cameron,[1]* C. M. Carollo,[1] P. Oesch,[1] M. C. Aller,[1] T. Bschorr,[1] P. Cerulo,[1]
H. Aussel,[2] P. Capak,[3,4] E. Le Floc'h,[2] O. Ilbert,[5] J.-P. Kneib,[5] A. Koekemoer,[6]
A. Leauthaud,[7] S. J. Lilly,[1] R. Massey,[3,8] H. J. McCracken,[9] J. Rhodes,[3,10] M. Salvato,[3]
D. B. Sanders,[11] N. Scoville,[3] K. Sheth,[3,4] Y. Taniguchi[12] and D. Thompson[3,13]

[1]*Department of Physics, Swiss Federal Institute of Technology (ETH Zurich), CH-8093 Zurich, Switzerland*
[2]*AIM, CNRS, Université Paris Diderot, Bât. 709, CEA-Saclay, 91191 Gif-sur-Yvette Cedex, France*
[3]*California Institute of Technology, MS 105-24, 1200 East California Boulevard, Pasadena, CA 91125, USA*
[4]*Spitzer Space Center, California Institute of Technology, Pasadena, CA 91125, USA*
[5]*Laboratoire d'Astrophysique de Marseille, CNRS, Université de Provence, 38 rue Frédéric Joliot-Curie, 13388 Marseille Cedex 13, France*
[6]*STScI, 3700 San Martin Drive, Baltimore, MD 21218, USA*
[7]*LBNL & BCCP, University of California, Berkeley, CA 94720, USA*
[8]*Institute for Astronomy, Royal Observatory, Edinburgh EH9 3HJ*
[9]*Institut d'Astrophysique de Paris, UMR 7095, CNRS, Université Pierre et Marie Curie, 98 bis Boulevard Arago, 75014 Paris, France*
[10]*Jet Propulsion Laboratory, MS 169-506, 4800 Oak Grove Drive, Pasadena, CA 91109, USA*
[11]*Institute for Astronomy, 2680 Woodlawn Drive, University of Hawaii, Honolulu, HI 96822, USA*
[12]*Research Center for Space and Cosmic Evolution, Ehime University, Bunkyo-cho 2-5, Matsuyama 790-8577, Japan*
[13]*LBT Observatory, University of Arizona, 933 North Cherry Avenue, Tucson, AZ 85721, USA*

ABSTRACT

We investigate the (large-scale) bar fraction in a *mass-complete* sample of $M > 10^{10.5}\,\mathrm{M_\odot}$ disc galaxies at $0.2 < z < 0.6$ in the Cosmological Evolution Survey (COSMOS) field. The fraction of barred discs strongly depends on mass, disc morphology and specific star formation rate (SSFR). At intermediate stellar mass ($10^{10.5} < M < 10^{11}\,\mathrm{M_\odot}$) the bar fraction in early-type discs is much higher, at all redshifts, by a factor of ~ 2, than that in late-type discs. This trend is reversed at higher stellar mass ($M > 10^{11}\,\mathrm{M_\odot}$), where the fraction of bars in early-type discs becomes significantly lower, at all redshifts, than that in late-type discs. The bar fractions for galaxies with low and high SSFRs closely follow those of the morphologically selected early- and late-type populations, respectively. This indicates a close correspondence between morphology and SSFR in disc galaxies at these earlier epochs. Interestingly, the total bar fraction in $10^{10.5} < M < 10^{11}\,\mathrm{M_\odot}$ discs is built up by a factor of ~ 2 over the redshift interval explored, while for $M > 10^{11}\,\mathrm{M_\odot}$ discs it remains roughly constant. This indicates that, already by $z \sim 0.6$, spectral and morphological transformations in the most massive disc galaxies have largely converged to the familiar Hubble sequence that we observe in the local Universe, while for intermediate-mass discs this convergence is ongoing until at least $z \sim 0.2$. Moreover, these results highlight the importance of employing mass-limited samples for quantifying the evolution of barred galaxies. Finally, the evolution of the barred galaxy populations investigated does not depend on the large-scale environmental density (at least, on the scales which can be probed with the available photometric redshifts).

Key words: galaxies: evolution – galaxies: formation – galaxies: structure.

1 INTRODUCTION

Numerous observational studies have demonstrated that large-scale stellar bars are remarkably common amongst local disc galaxies (e.g. de Vaucouleurs et al. 1991; Eskridge et al. 2000; Menéndez-Delmestre et al. 2007; Aguerri, Méndez-Abreu & Corsini 2009), and that a substantial population of barred discs exists out to at least redshift unity (e.g. Abraham et al. 1999; Elmegreen, Elmegreen & Hirst 2004; Jogee et al. 2004; Elmegreen et al. 2007; Sheth et al. 2008). Quantifying the fraction of barred discs as a function of redshift, and its dependence on fundamental galaxy properties, is an

*E-mail: cameron@phys.ethz.ch

essential step towards understanding galaxy formation in a cosmological context. Importantly, large-scale bars serve as signposts of massive, dynamically cold discs (Athanassoula & Sellwood 1986), constraining their epoch of formation (Sheth et al. 2008). Moreover, bars are key drivers of secular evolution in their host galaxies, redistributing angular momentum, enhancing nuclear star formation and building pseudo-bulges (e.g. Lynden-Bell & Kalnajs 1972; Combes et al. 1990; Knapen et al. 1995; Carollo et al. 1997, 2001, 2002, 2007; Carollo 1999; Sheth et al. 2000; Kormendy & Kennicutt 2004; Sheth et al. 2005; Debattista et al. 2006; Foyle, Rix & Zibetti 2009; Comerón et al. 2010).

A number of recent studies have examined the disc galaxy bar fraction for luminosity-selected samples at intermediate to high redshifts in the field (e.g. Jogee et al. 2004; Sheth et al. 2008), in clusters (Marinova et al. 2009) or both (Barazza et al. 2009). Jogee et al. (2004) recovered a constant bar fraction out to redshift unity in the Galaxy Evolution from Morphologies and SEDs (GEMS) survey for disc galaxies at $M_V \leq -19.3$ and -20.6 mag. Conversely, for galaxies at L_V^* ($M_V^* = -21.7$ mag at $z = 0.9$) and brighter in the Cosmological Evolution Survey (COSMOS), Sheth et al. (2008) identified a build-up of the barred population over the same epoch. Marinova et al. (2009) and Barazza et al. (2009) have identified a minimal dependence of the bar fraction on environment (see also Méndez-Abreu, Sánchez-Janssen & Aguerri 2010), except perhaps in cluster centres, where bar formation appears to be enhanced. Both studies also recovered a rise in the bar fraction towards later morphological types, or bluer, increasingly disc-dominated systems, while Sheth et al. (2008) recovered an enhanced bar fraction in redder, increasingly bulge-dominated systems at high redshifts. However, care must be taken when comparing these results due to the different luminosity limits adopted (e.g. Marinova et al. 2009 and Barazza et al. 2009 sampled faint discs down to $M_V \leq -18$ mag at $z \sim 0.165$ and $M_V \leq -20$ mag at $0.4 < z < 0.8$, respectively). Interestingly, the highest bar fraction found by Marinova et al. (2009) was 75 ± 11 per cent for clumpy discs with distinct bulges at high luminosities ($-21 < M_V < -20$ mag). A further complication is introduced by the various methods of disc selection employed, whether spectral energy distribution (SED) fit type and visual inspection (Sheth et al. 2008), visual inspection alone (Barazza et al. 2009), or colour, global Sérsic index and visual inspection (Marinova et al. 2009).

In the light of recent evidence that galaxy evolutionary histories are tied closely to total stellar mass (Bundy, Ellis & Conselice 2005; Baldry et al. 2006; Bolzonella et al. 2009; Tasca et al. 2009; Kovac et al. 2010), the further study of evolution in mass-limited samples is a crucial step forward to undertake. In this paper we quantify the bar fraction at intermediate to high redshifts, at fixed stellar mass, using a sample of 916 morphologically classified disc galaxies in the COSMOS field. Specifically, we study the dependence of the (large-scale) bar fraction on detailed morphological type (early- or late-type discs), specific star formation rate (SSFR) and large-scale environmental density.

The outline of this paper is as follows. In Section 2 we review the COSMOS data set employed in this work, and describe our sample selection. In Section 3 we explain our bar detection procedure and method of accounting for selection biases. In Section 4 we present our results and in Section 5 we discuss their implications for galaxy formation scenarios. The construction and bar fraction analysis of a complementary sample of local Universe disc galaxies in the Sloan Digital Sky Survey (SDSS) is described in Appendix A. We adopt a cosmological model with $\Omega_\Lambda = 0.75$, $\Omega_M = 0.25$ and $h = 0.7$, and all magnitudes are quoted in the AB system throughout.

2 DATA SET AND ANCILLARY MEASUREMENTS

We use the COSMOS data set (Scoville et al. 2007), consisting of ground-based and space-based, multiwavelength imaging of an ~ 2 deg^2 equatorial field. In particular, as the starting point for our sample definition, we adopt the *I*-band source catalogue of Leauthaud et al. (2007) extracted from the COSMOS ACS *I*-band imaging frames (Koekemoer et al. 2007), consisting of 156 748 sources limited down to $I_{AB} = 26.6$ mag. Careful artefact and star removal was performed to improve the robustness of this catalogue, and computation of photometric redshifts was attempted for 111 141 of these sources flagged as galaxies (i.e. removing stars and junk).

11 photometric bands covering the wavelength range between the COSMOS Canada–France–Hawaii Telescope (CFHT) *u* and the *Spitzer* 4.5-μm band (see Capak et al. 2007; Sanders et al. 2007) were used to derive these photometric redshifts using our own Zurich Extragalactic Bayesian Redshift Analyzer (ZEBRA[1]) code (Feldmann et al. 2006). To this end, we used galaxies with secure spectroscopic redshifts from the zCOSMOS survey (Lilly et al. 2007, 2009) and modified with ZEBRA our set of empirical templates (Coleman, Wu & Weedman 1980; Kinney et al. 1996) to account for systematic, template-dependent mismatches with the photometric SEDs of the sample galaxies. An acceptable template match was able to be identified for all but 1695 of the 111141 input sources (a 1.5 per cent failure rate). The resulting photometric redshifts have an uncertainty of $\Delta(z)/(1 + z) \sim 0.023(1 + z)$ down to $I < 22.5$ mag, as directly tested with available spectroscopic redshifts from zCOSMOS. We estimated the photometric redshift accuracy at magnitudes fainter than $I = 22.5$ mag by dimming the photometry of zCOSMOS galaxies down to $I = 24$ mag; this results in an uncertainty of $0.039(1 + z)$. As a cross-check, we also used the photometric redshifts of Ilbert et al. (2009), which became available in the meantime. These are based on a photometric catalogue of the COSMOS survey with 30 photometric bands including also narrow- and intermediate-band filters, and the effects of both dust extinction and emission lines on template fitting were accounted for carefully during their computation. Based on the comparison with the spectroscopic redshifts of the $I < 22.5$ mag zCOSMOS sample, the dispersion of the Ilbert et al. (2009) photo-*z* catalogue is $\sim 0.007(1+z)$ [and $\sim 0.012(1+z)$ down to $I = 24$ mag; Ilbert et al. 2009]. Owing to the use of a much larger number of photometric passbands, the Ilbert et al. (2009) redshifts have a higher accuracy than our ZEBRA estimates. The advantage of the latter, however, is that they were derived by ourselves, and we are thus fully aware of their caveats and limitations. We therefore take the conservative strategy to use both versions of the COSMOS photo-*z*s in our analysis, as a means to identify any systematic uncertainty associated with the photometric redshift estimates.

In order to estimate stellar masses from the photometric data, we used a newly developed, non-public extension of our ZEBRA code, ZEBRA+, which estimates galaxy physical parameters, such as stellar masses, by fitting synthetic stellar population model SEDs to the galaxy broad-band photometry (cf. Fontana et al. 2004; Pozzetti et al. 2007; Marchesini et al. 2009). As in ZEBRA's maximum likelihood mode, the best-fitting SED and its normalization, are computed by minimizing the χ^2 between the observed and template fluxes. Additionally, ZEBRA+ includes reddening of the input SEDs with

---

[1] The code is publicly available under the following URL: www.exp-astro.phys.ethz.ch/ZEBRA

a variety of dust laws, when required. Using the zCOSMOS 10 k sample Bolzonella et al. (2009) have demonstrated a level of uncertainty of $\sigma_{\log M} \approx 0.20$ arising from the choices of SED template and dust extinction law for stellar masses derived via SED fitting to the COSMOS photometric data. This is consistent with the scatter of $\sigma_{\log M} \approx 0.27$ between our ZEBRA+ stellar mass estimates and those from the publicly available catalogue of Pannella et al. (2009) for galaxies well matched in both position (centroid difference less than 2×10^{-5} arcsec) and photometric redshift [$|z_{ZEBRA} - z_{Pannella}| < 0.02\,(1 + z_{ZEBRA})$]. Details for ZEBRA+, including a further investigation into the relevant uncertainties, are given in Oesch et al. (in preparation; see also Oesch et al. 2010). An acceptable synthetic template match for computation of stellar masses was able to be identified for all but 7033 of the 109 446 galaxies with estimated photometric redshifts (a 6 per cent failure rate). We stress that our results remain unchanged when using either of the two photo-z catalogues; furthermore, the resulting uncertainties in the stellar mass and star formation rate estimates are negligible. A total of 32 840 galaxies were identified with photometric redshifts in the range $0.2 < z < 0.6$ examined in this study, of which 3519 are above the adopted mass limit of $M > 10^{10.5}\,M_\odot$.

Star formation rates were computed based upon each galaxy's total infrared (IR) luminosity [L_{IR}; derived from the Multiband Imaging Photometer for Spitzer (MIPS) detections at 24 µm, LeFloc'h et al. (2009), down to a flux limit of 0.15 mJy, using the templates of Rieke et al. (2009)] and total ultraviolet (UV) luminosity (L_{UV}; estimated by interpolating the observed SEDs to 2800 Å). Specifically, we adopt the relation SFR $= 9.8 \times 10^{-11}(L_{IR} + 2.2L_{UV})\,M_\odot\,yr^{-1}$ from Bell et al. (2005). The total uncertainties in our SFR estimates are ∼0.4 dex, given the ∼0.3 dex intrinsic scatter about this relation (Bell et al. 2005) and the ∼0.3 dex uncertainty on the estimation of UV luminosities from our SED template fits. Environmental densities are sourced from Scoville et al. (2007) catalogue of (large-scale) surface densities for COSMOS galaxies in fixed redshift intervals.

Galaxy morphologies were obtained with an upgraded version of the Zurich Estimator of Structural Types (ZEST; Scarlata et al. 2007), known as ZEST+ (Carollo et al., in preparation). Relative to its predecessor, ZEST+ includes additional measurements of non-parametric morphological indices for characterizing both structure and substructure. Moreover, ZEST+ offers a support vector machine (SVM) classification (adopted herein), as well as a principal component analysis (PCA) scheme for consistency with the earlier ZEST. The ZEST+ SVM classifies galaxies in seven morphological types located in specific regions of the 6D space of concentration, asymmetry, clumpiness, M_{20}, Gini coefficient and ellipticity. The different types were visually inspected to ensure a broad equivalence with the following Hubble types: E, S0–Sa, Sb, Sc, Sd and Irr (with the Irr types divided into two classes, 'concentrated' and 'non-concentrated', according to the value of the concentration index). As a result of visual inspection of the 3519 galaxies in our sample at $0.2 < z < 0.6$ and $M > 10^{10.5}\,M_\odot$, a total of 36 Irr, 14 S0–Sa and 33 spiral (Sa–Sb to Sc–Sd) systems were identified as 'catastrophic' misclassifications and were manually reassigned to their respective types. The two most frequent causes of such 'catastrophic' misclassifications were the presence of bright, overlapping neighbours and/or strong dust lanes (see Sargent et al. 2010 for a detailed study of the impact of dust on discs in COSMOS), which can bias recovery of the quantitative morphological indices used as input to the SVM analysis module. Regarding the reliability of ZEST+ output in general, calibrations performed by Scarlata et al. (2007) using the original ZEST code to classify real COSMOS galaxies show that down to $I = 24$ mag the misclassification rate is at most ∼30 per
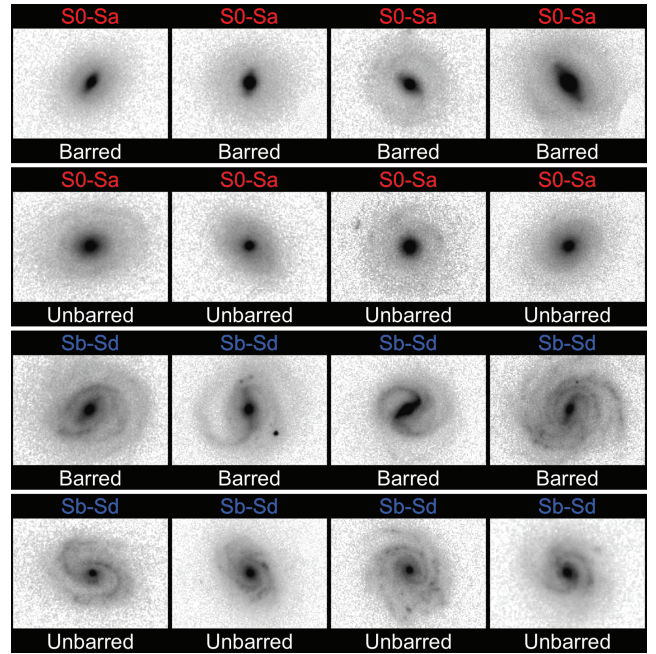

Figure 1. Example (*HST* ACS *I*-band) postage stamp images of both early-type (*top two rows*) and late-type (*bottom two rows*), barred and unbarred galaxies from our sample of 916 COSMOS discs at $0.2 < z < 0.6$, $M > 10^{10.5}\,M_\odot$, and $e < 0.3$. The width of each of these postage stamps was adjusted within a range of 3.3–6.3 arcsec in angular size to best emphasize the morphological details of each system.

cent for ellipticals incorrectly identified as early- and intermediate-type discs in the lowest signal-to-noise ratio (S/N) bin. As ZEST+ features substantially improved algorithms for computation of the relevant quantitative morphological indices relative to the original ZEST, we are confident that the ZEST+ morphological classifications are even more reliable than those of ZEST.

The end result of our classification process was a final sample of 2820 disc galaxies (morphological type between S0–Sa and Sc–Sd), of which 916 have ellipticities (e) less than 0.3 (equivalent to disc inclination less than 45°). Example [*Hubbe Space Telescope* (*HST*) Advanced Camera for Surveys (*ACS*) *I* band] postage stamp images of both early- and late-type, barred and unbarred systems from our final sample of 916 COSMOS discs at $0.2 < z < 0.6$, $M > 10^{10.5}\,M_\odot$ and $e < 0.3$ are presented in Fig. 1.

3 METHOD

3.1 Bar detection

Barred galaxies in our sample were identified as follows. First, the ellipse package in IRAF was used to recover the elliptical isophote profile of each galaxy from its ACS *I*-band image. Specifically, ellipse was run repeatedly for each galaxy, varying the initial guesses of object position, semimajor axis, ellipticity and position angle until a robust fit was recovered down to the level of sky noise (cf. Regan & Elmegreen 1997; Laine et al. 2002; Menéndez-Delmestre et al. 2007). If a robust fit could not be identified with a single combination of initial parameter guesses (<5 per cent of cases), the profile was constructed piecewise from the robust sections of two or more fitting attempts. Pixels within 2.5 times the Kron radius of any nearby neighbours were excluded from the fitting process.

All galaxies with profiles displaying a monotonic increase in ellipticity of $e_{min} \geq 0.4$ with a subsequent drop of at least $\Delta e \geq 0.1$ were flagged as candidate barred systems. The threshold of $e_{min} \geq 0.4$ was chosen to replicate the selection of strong galaxy bars made by Jogee et al. (2004) and Sheth et al. (2008). However, unlike these other studies, we did not reject candidate barred systems based on a further criterion of isophote position angle change at the bar end. Rather, the final selection of barred galaxies was performed via visual inspection of the candidates, thereby maximizing the completeness of our bar sample (i.e. allowing for detection of those galaxies in which, by chance, the uncorrelated bar and disc position angles are closely aligned; cf. Menéndez-Delmestre et al. 2007). In total, 213 (67 per cent) of our 320 candidate barred systems (23 per cent of the entire disc galaxy sample) were thereby confirmed as barred. A further 23 barred candidates that were ultimately rejected were noted as 'ambiguous' cases (e.g. the 'bar' morphology was perhaps more consistent with that of a lens or truncated inner disc). Example (*HST* ACS *I*-band) postage stamp images of both early- and late-type, barred and unbarred galaxies from our final sample of 916 COSMOS discs at $0.2 < z < 0.6$, $M > 10^{10.5}$ M$_\odot$ and $e < 0.3$ are presented in Fig. 1.

3.2 Accounting for selection effects

Completeness limits on bar detection given the isophotal ellipticity criteria described above were estimated via artificial galaxy simulations. Both early- and late-type barred galaxy models were constructed from three components: a Sérsic bulge, a (truncated) Sérsic bar and an exponential disc. The properties of each model were chosen to be consistent with the observed properties of barred galaxies in the local Universe (Elmegreen et al. 1996; Laurikainen et al. 2007; Gadotti 2008; Weinzirl et al. 2009), and are listed in Table 1. The use of three different early-type models was necessary to replicate the variety of structural types observed amongst local S0 and Sa systems (e.g. Balcells et al. 2003). Importantly, the models adopted span a wide range of bulge Sérsic indices ($1 \leq n \leq 4$) and bulge-to-total flux ratios ($0.1 \leq$ B/T ≤ 0.6), and thus encompass the entire parameter space observed for massive local disc galaxies.

For all models we adopt a bar ellipticity of $e = 0.6$ as this represents a lower limit on the intrinsic bar ellipticities (e) typically recovered for massive disc galaxies in 2D bulge–bar–disc structural decomposition studies (e.g. Gadotti 2008). The lower the intrinsic ellipticity of the bar, the lower the mean surface brightness (at a given Bar/T), so it follows that that low-ellipticity bars will

Table 1. Key model parameters for artificial galaxy simulations of bar detection completeness.

#	Type	B/T	Bar/T	R_e/h [a]	n [a]	n_{bar} [a]	L_{bar}/h [a]
1	Early	0.4	0.15	0.2	4.0	0.7	1.15
2	Early	0.2	0.15	0.2	2.5	0.7	1.15
3	Early	0.6	0.15	0.2	4.0	0.7	1.15
4	Late	0.1	0.10	0.1	1.0	0.9	0.90

[a]These symbols refer to the effective radius (R_e), Sérsic index (n) and truncation length (L) of the generalized 2D Sérsic profile (cf. Aguerri et al. 2009; Graham & Driver 2005) employed for the model bulge and bar components, while h is the scalelength of the underlying exponential disc. In all cases we adopt ellipticities (e) of $e = 0$ and $e_{bar} = 0.6$, and shape parameters (c) of $c = 2$ (elliptical isophotes) and $c_{bar} = 2.4$ (boxy isophotes), for the bulge and bar, respectively. Note that in each artificial galaxy image generated the bar length is scaled relative to the projection of the disc.

be most sensitive to surface brightness dependent detection biases. Moreover, the lower the intrinsic bar ellipticity, the more sensitive will the system be to size-dependent detection biases caused by the 'rounding' of bar isophotes by the point spread function (PSF). Hence, by using a 'lower limit' bar ellipticity of $e = 0.6$ in all models we best expose the limits of our detection routine, and thereby identify safely conservative selection limits.

Artificial galaxy images for each type of model were generated and convolved with a Gaussian PSF of 0.12-arcsec (4 pixels) full width at half-maximum (FWHM), then degraded to the noise level of the COSMOS ACS *I*-band imaging. A total of 1960 images were constructed for each model in a grid of total galaxy magnitudes and disc scalelengths spanning $I = 17$–24 mag and $h = 0.15$–3 arcsec (5–100 pixels), respectively. 10 instances of each model were generated at each grid point with random disc inclinations ranging $0°$–$45°$, and random component position angles (with the bar size scaled relative to the projection of the disc). These images were run through our candidate bar detection pipeline, and the results are plotted as a function of total galaxy magnitude and total half-light radius (more easily comparable against observations than disc scalelength) in Fig. 2.

These simulations indicate a high bar detection completeness for most galaxies in our sample, supposing a mix of early- and late-type discs equivalent in structure to our models #1, #2 and #4 (see Table 1). Although simulations with early-type model #3 revealed that our detection procedure is unlikely to discover bars in any severely bulge-dominated systems (B/T $\gtrsim 0.6$), high-resolution imaging studies indicate a negligible large-scale bar fraction for such galaxies in any case (e.g. Laurikainen et al. 2007; Weinzirl et al. 2009). Comparing the distribution of ZEST+ classified discs with $M > 10^{10.5}$ M$_\odot$ and $i < 45°$ at $0.2 < z < 0.6$ in the COSMOS field against the model completeness limits at low surface brightness (for models #1, #2 and #4, see Fig. 2) reveals that bar detection in our sample is not surface brightness limited. In particular, there are very few galaxies with observed magnitudes and half-light radii approaching these limits, even after accounting for the systematic biases at low S/N inherent in the Kron-style measurements employed here (cf. Cameron & Driver 2009). However, the limit for bar detection in galaxies with small apparent half-light radii ($R_e \sim 0.33$ arcsec) is significant and must be considered in our analysis.

To ensure a uniform detection completeness of barred discs at all redshifts we exclude from our subsequent analysis all galaxies smaller than the physical size represented by this apparent size limit at the highest redshifts explored here (i.e. $R_{e,lim} = 2.2$ kpc at $z = 0.6$). This cut removes 283 (~ 31 per cent) of our initial sample of 916 COSMOS discs, including 30 bars confidently detected in (primarily early-type) galaxies with $R_e \sim 1.5$–2.2 kpc at $z \lesssim 0.45$. Hence, we can confirm that bars are observed to exist in compact discs at these intermediate redshifts, but note that the evolution of this population cannot be robustly constrained with the available data. Therefore, we emphasize that the results presented in this study concern intermediate-to-large discs ($R_e > 2.2$ kpc) only.

4 RESULTS

In Fig. 3 we present the (strong) bar fraction of ZEST+ classified disc galaxies with $M > 10^{10.5}$ M$_\odot$, $i < 45°$ and $R_e > 2.2$ kpc in the COSMOS field in redshift bins of $0.2 < z < 0.3, 0.3 < z < 0.4, 0.4 < z < 0.5$ and $0.5 < z < 0.6$. Two key stellar mass regimes are explored: intermediate mass ($10^{10.5} < M < 10^{11}$ M$_\odot$) and high mass ($M > 10^{11}$ M$_\odot$). Within each mass regime we further explore
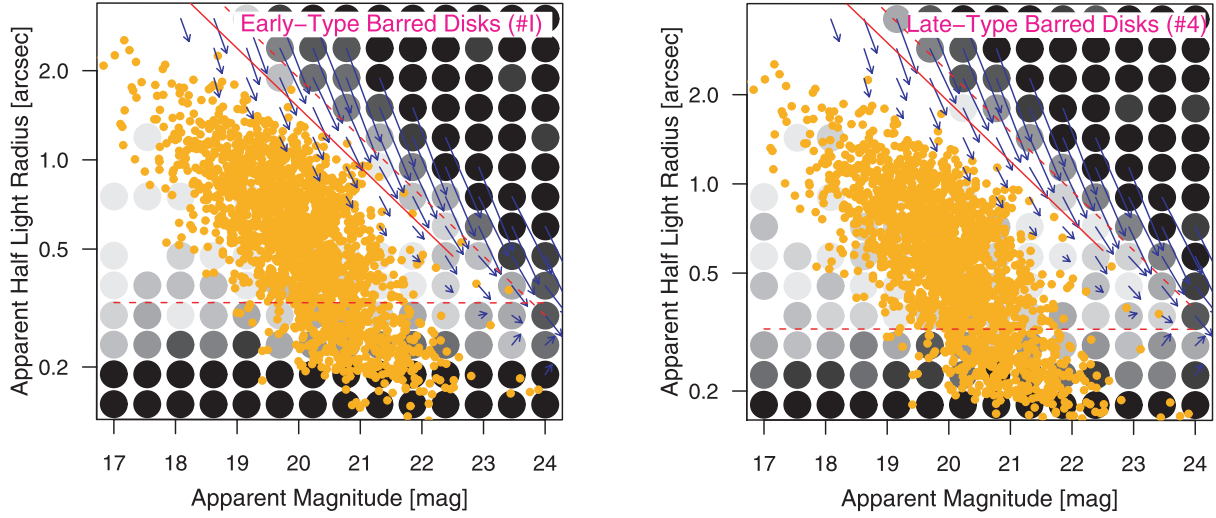
Figure 2. The recoverability of bars in the COSMOS ACS *I*-band imaging for early-type (*left*) and late-type (*right*) model discs at low inclination ($i < 45°$) as derived via artificial galaxy simulations. The detection completeness of input bars identified via our isophotal ellipse-fitting procedure in each bin of intrinsic (i.e. input) apparent magnitude and half-light radius is indicated by the large grey-shaded circles on a scale from white representing 100 per cent completeness to black representing zero per cent completeness. The effective limits on (intrinsic) apparent size and surface brightness for high detection completeness are highlighted by dashed, red lines. Blue arrows indicate the mean errors on the measurement of (Kron-style) galaxy magnitudes and sizes towards low surface brightnesses, and red, solid lines mark boundaries within which galaxies are no longer scattered in (due to measurement errors) from regions of low detection completeness. Finally, the orange data points reveal the observed distribution of ZEST+ classified disc galaxies with $M > 10^{10.5}$ M$_\odot$ and $i < 45°$ at $0.2 < z < 0.6$ in the COSMOS field. Note that only the results for simulations corresponding to our models #1 and #4 (see Table 1) are displayed here; the results for model #2 were nearly identical to those for model #1, while almost no bars were recovered for model #3 (see the discussion in Section 3.2).
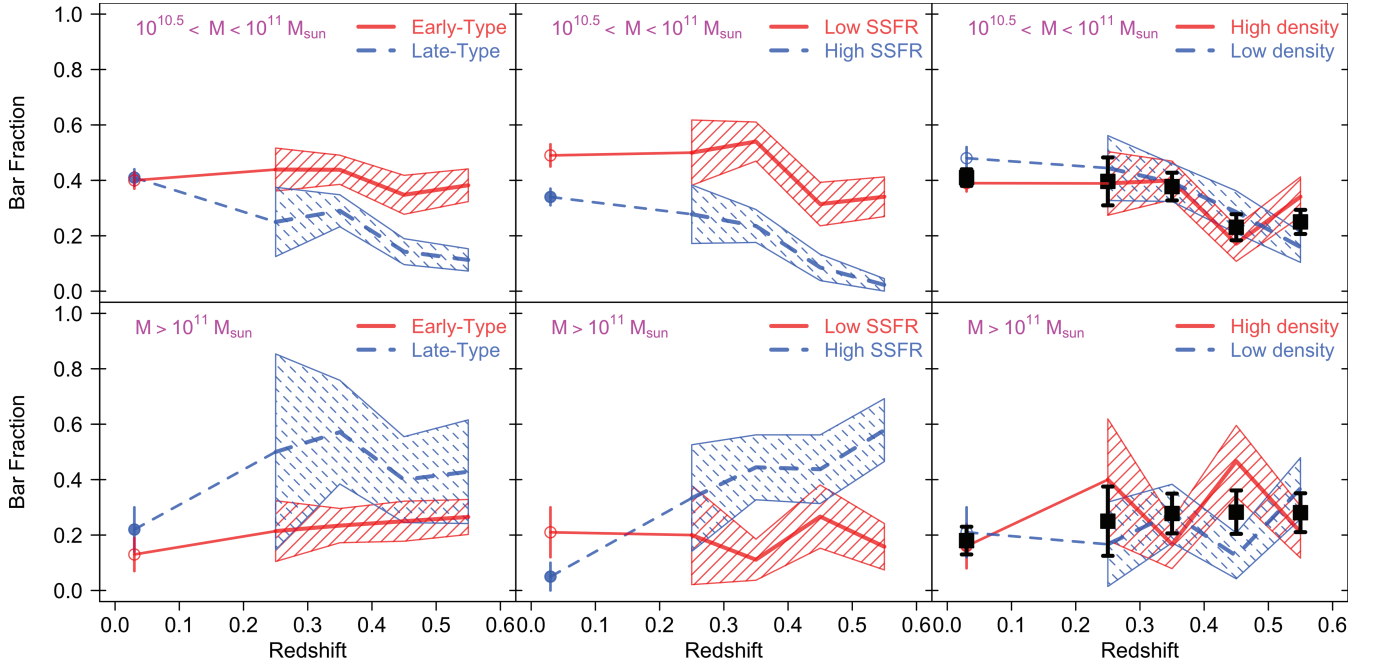

Figure 3. The redshift evolution of the bar fractions of ZEST+ classified disc galaxies with $M > 10^{10.5}$ M$_\odot$, $i < 45°$, and $R_e > 2.2$ kpc at $0.2 < z < 0.6$ in the COSMOS field subdivided by stellar mass, morphological type, SSFR and environmental density. Galaxies at intermediate stellar mass ($10^{10.5} < M < 10^{11}$ M$_\odot$) are shown on the top row, while those at high stellar mass ($M > 10^{11}$ M$_\odot$) are shown on the bottom row. The left-hand column displays the bar fraction evolution by ZEST+ morphological type for early- and late-type discs. The middle and right-hand columns display the bar fraction evolution by SSFR and (large-scale) environmental density, respectively, for the lowest and highest thirds of the population in each mass and redshift bin. In each panel the thick red and blue lines indicate the bar fractions of the relevant populations, and the corresponding uncertainties are revealed by the cross-hatched areas. The black squares and error bars overlaid on the plots by density indicate the total disc galaxy bar fraction in each redshift bin. Note the lack of evolution at $M > 10^{11}$ M$_\odot$, and the net evolution below this mass scale. The local Universe bar fractions marked at $z = 0.03$ indicate the values measured in our low-redshift ($0.02 < z < 0.04$) SDSS comparison sample selected and analysed as described in Appendix A.

Table 2. Bar fractions by mass, morphology, SSFR and environmental density in COSMOS at $0.2 < z < 0.6$.

Redshift	Stellar mass[a]	Morphological type	Specific star formation rate[a]	Environmental density[a]
$0.2 < z < 0.3$	Intermediate	Early-type: $f_{bar} = 0.44 \pm 0.08$	Low SSFR: $f_{bar} = 0.50 \pm 0.11$	High density: $f_{bar} = 0.44 \pm 0.11$
$0.2 < z < 0.3$	Intermediate	Late-type: $f_{bar} = 0.25 \pm 0.13$	High SSFR: $f_{bar} = 0.27 \pm 0.11$	Low density: $f_{bar} = 0.38 \pm 0.11$
$0.2 < z < 0.3$	High	Early-type: $f_{bar} = 0.21 \pm 0.11$	Low SSFR: $f_{bar} = 0.20 \pm 0.18$	High density: $f_{bar} = 0.16 \pm 0.15$
$0.2 < z < 0.3$	High	Late-type: $f_{bar} = 0.50 \pm 0.35$	High SSFR: $f_{bar} = 0.33 \pm 0.19$	Low density: $f_{bar} = 0.40 \pm 0.21$
$0.3 < z < 0.4$	Intermediate	Early-type: $f_{bar} = 0.44 \pm 0.05$	Low SSFR: $f_{bar} = 0.54 \pm 0.07$	High density: $f_{bar} = 0.39 \pm 0.07$
$0.3 < z < 0.4$	Intermediate	Late-type: $f_{bar} = 0.29 \pm 0.06$	High SSFR: $f_{bar} = 0.24 \pm 0.06$	Low density: $f_{bar} = 0.40 \pm 0.07$
$0.3 < z < 0.4$	High	Early-type: $f_{bar} = 0.23 \pm 0.06$	Low SSFR: $f_{bar} = 0.11 \pm 0.07$	High density: $f_{bar} = 0.28 \pm 0.10$
$0.3 < z < 0.4$	High	Late-type: $f_{bar} = 0.57 \pm 0.18$	High SSFR: $f_{bar} = 0.44 \pm 0.12$	Low density: $f_{bar} = 0.17 \pm 0.09$
$0.4 < z < 0.5$	Intermediate	Early-type: $f_{bar} = 0.35 \pm 0.07$	Low SSFR: $f_{bar} = 0.31 \pm 0.07$	High density: $f_{bar} = 0.29 \pm 0.07$
$0.4 < z < 0.5$	Intermediate	Late-type: $f_{bar} = 0.14 \pm 0.05$	High SSFR: $f_{bar} = 0.08 \pm 0.05$	Low density: $f_{bar} = 0.17 \pm 0.06$
$0.4 < z < 0.5$	High	Early-type: $f_{bar} = 0.25 \pm 0.07$	Low SSFR: $f_{bar} = 0.27 \pm 0.11$	High density: $f_{bar} = 0.13 \pm 0.08$
$0.4 < z < 0.5$	High	Late-type: $f_{bar} = 0.40 \pm 0.15$	High SSFR: $f_{bar} = 0.44 \pm 0.12$	Low density: $f_{bar} = 0.46 \pm 0.13$
$0.5 < z < 0.6$	Intermediate	Early-type: $f_{bar} = 0.38 \pm 0.06$	Low SSFR: $f_{bar} = 0.34 \pm 0.07$	High density: $f_{bar} = 0.16 \pm 0.05$
$0.5 < z < 0.6$	Intermediate	Late-type: $f_{bar} = 0.11 \pm 0.04$	High SSFR: $f_{bar} = 0.03 \pm 0.03$	Low density: $f_{bar} = 0.34 \pm 0.07$
$0.5 < z < 0.6$	High	Early-type: $f_{bar} = 0.26 \pm 0.06$	Low SSFR: $f_{bar} = 0.16 \pm 0.08$	High density: $f_{bar} = 0.37 \pm 0.11$
$0.5 < z < 0.6$	High	Late-type: $f_{bar} = 0.43 \pm 0.19$	High SSFR: $f_{bar} = 0.58 \pm 0.11$	Low density: $f_{bar} = 0.21 \pm 0.09$

[a]Here we define intermediate stellar mass as $10^{10.5} < M < 10^{11}\,M_\odot$ and high stellar mass as $M > 10^{11}\,M_\odot$, and we identify the low and high SSFR (or environmental density) populations as the lower and upper thirds of the SSFR (or environmental density) distribution in each mass and redshift bin (as explained in Section 4). The COSMOS disc sample examined is also restricted to systems with $e < 0.3$ and $R_e > 2.2$ kpc as described in Section 3.2.

the dependence of bar fraction on (zEST+ classified) morphological type (early-type versus late-type), specific star formation rate and (large-scale) environmental density. For the purposes of exploring the latter two redshift dependencies we identify the lower and upper thirds of the population in each parameter in each mass and redshift bin. We also note that the error bars shown in Fig. 3 reflect the Poisson uncertainties only; cosmic variance potentially contributes an additional ∼13 per cent uncertainty for populations of this number density in the volume sampled (cf. Trenti & Stiavelli 2008). The bar fractions and statistical uncertainties for each redshift, mass, morphology, SSFR and environmental density bin measured here (and shown in Fig. 3) are compiled in Table 2 for reference.

At intermediate stellar mass the mean bar fraction of early-type discs ($f_{bar} = 0.42 \pm 0.05$) is much higher than that of late-type discs ($f_{bar} = 0.19 \pm 0.03$) over the redshift interval explored. However, at high stellar mass this trend is reversed with early-type discs less frequently barred ($f_{bar} = 0.20 \pm 0.04$) than late-type discs ($f_{bar} = 0.43 \pm 0.07$). The bar fractions of galaxies with the lowest and highest specific star formation rates at both mass regimes closely follow the trends evident in the morphologically selected early- and late-type populations, respectively, reflecting a close relationship between disc morphology and star formation rate at these epochs. The bar fractions by large-scale environmental density reveal no relationship between the frequency of bars and environment at fixed mass. However, we caution that the environmental densities from Scoville et al. (2007) used here are based on photometric redshifts and averaged over >100 Mpc scales. Hence, we are unable to confirm a null dependence of the bar fraction on density down to group scales with this data set. Finally, the total bar fraction is observed to build up by a factor of ∼2 between $z \sim 0.6$ and 0.2 at intermediate stellar mass, but at high stellar mass a null evolution scenario is favoured.

The local Universe bar fractions measured in a complementary sample of SDSS discs at $0.02 < z < 0.04$ described in Appendix A are also shown in Fig. 3 for comparison. At intermediate stellar mass

these low-redshift data points confirm that the bar fraction in early-type discs remains constant, or even exhibits a slight decline, from $z \sim 0.2$ to 0 while assembly of the late-type barred disc population continues to the present day. At high stellar masses these local Universe results are consistent with the null evolution of the early-type bar fraction since $z \sim 0.6$ evident in the COSMOS data set. At face value, the bar fraction in late-type discs at high mass in the SDSS at $0.02 < z < 0.04$ is much lower than that at $0.2 < z < 0.6$ measured in COSMOS; however, the statistical uncertainties are rather large due to the low number density of this galaxy population. Indeed, there is a clear dependence of the total bar fraction on mass in both our low- and high-redshift samples, supporting our main conclusions.

5 DISCUSSION

Several observational studies indicate that the large/massive disc galaxy population has reached a mature state by redshift unity. These studies include the null evolution in the disc galaxy mass–size relation (Barden et al. 2005), the size function of large discs (Lilly et al. 1998; Cameron & Driver 2007; Sargent et al. 2007), the *B*-band Tully–Fisher relation for massive discs (Ziegler et al. 2002), and the morphological mix of massive galaxies (Oesch et al. 2010) since $z \sim 0.7$–1, as well as the relative paucity of highly disturbed and highly diffuse galaxies at $z \lesssim 1$ (Conselice et al. 2004). Our work adds an important additional piece of information. There exist substantial populations of barred early- and late-type discs – whether defined by morphology or SSFR – at $M > 10^{11}\,M_\odot$ out to $z \sim 0.6$. At such high stellar masses the fractions of barred discs in each of these galaxy classes remain roughly constant over the ∼3.3 Gyr that separate the $z \sim 0.6$ from the $z \sim 0.2$ epochs. Thus, already at the intermediate redshifts explored in our study, spectral and morphological transformations within the most massive disc galaxies have largely converged, to such a level of detail, to the familiar Hubble sequence that we observe in the local Universe.

In contrast, at intermediate stellar mass ($10^{10.5} < M < 10^{11}$ M$_\odot$) there is a substantial build-up in the bar fractions of early- and late-type discs, and of the total disc population (by a factor of $\sim$2), over the past $\sim$3.3 Gyr of cosmic time. At such intermediate-mass scales, therefore, the disc galaxy population – and the disc galaxy sector of the Hubble sequence – continues structural evolution until at least $z \sim 0.2$. The preference for (large-scale) bars in intermediate-mass galaxies to reside in early-type discs – a trend also noted by Sheth et al. (2008) in their analysis of the COSMOS field – is perhaps a reflection of their earlier formation times compared to late-type discs of similar mass, i.e. these galaxies have evolved for longer in a dynamical state conducive to bar formation.

Interestingly, as the bar fraction reveals no dependence on large-scale environmental density at fixed mass, it would appear that any enhancement in the minor merger rate with environment (e.g. Heiderman et al. 2009) at these mass scales and redshifts does not lead to significant disc heating (cf. Hopkins et al. 2008), which could strongly impede bar formation (Athanassoula & Sellwood 1986). Although, an increase in the rate of tidally triggered bar formation in dense environments could also be masking this effect. We stress, however, that the 'environment' in our analysis, based on photometric redshifts, is averaged over >100 Mpc scales. The study of the bar fraction as a function of the group environment at early epochs is an important open question that we are exploring using the zCOSMOS group catalogue of Knobel et al. (2009). Moreover, given the importance of the group environment in determining the properties of local galaxies (e.g. Robotham, Phillipps & de Propris 2010), we will also soon be using the ZENS data set (Carollo et al., in preparation) to construct a key benchmark for the barred galaxy fraction in local groups (Cameron et al., in preparation).

Finally, our study also reveals the importance of investigating the evolution of barred galaxies at fixed stellar mass: this provides evidence for a substantial change in the relative fractions of bars in early- and late-type discs, and in the evolution of the total bar fraction, when stellar mass straddles across the 'critical' mass scale of $\sim10^{11}$ M$_\odot$. The close relationship between galaxy evolutionary histories and stellar mass has also been demonstrated recently via studies of local galaxy morphologies (Bundy et al. 2005) and colours (Baldry et al. 2006), as well as in high-redshift samples (Bolzonella et al. 2009; Tasca et al. 2009; Kovac et al. 2010). We therefore highlight the importance of constructing even larger, mass-limited disc galaxy samples at low and high redshifts for improving our understanding of bar formation – an endeavour that will be much assisted by various ground-based (UKIDSS, VIKING) and space-based (GOODS-ERS, HUDF09) near-infrared imaging surveys now under way, and their successors.

REFERENCES

Abraham R. G., Merrifield M. R., Ellis R. S., Tanvir N. R., Brinchmann J., 1999, MNRAS, 308, 569
Aguerri J. A. L., Méndez-Abreu J., Corsini E. M., 2009, A&A, 495, 491
Athanassoula E., Sellwood J. A., 1986, MNRAS, 221, 213
Balcells M., Graham A. W., Domínguez-Palmero L., Peletier R. F., 2003, ApJ, 582, L79
Baldry I. K., Balogh M. L., Bower R. G., Glazebrook K., Nichol R. C., Bamford S. P., Budavari T., 2006, MNRAS, 373, 469
Barazza F. D. et al., 2009, A&A, 497, 713
Barden M. et al., 2005, AJ, 635, 959
Bell E. et al., 2005, ApJ, 625, 23
Bolzonella M. et al., 2009, preprint (arXiv:0907.0013)
Brinchmann J., Charlot S., White S. D. M., Tremonti C., Kauffmann G., Heckman T., Brinkmann J., 2004, MNRAS, 351, 1151
Bundy K., Ellis R. S., Conselice C. J., 2005, ApJ, 625, 621
Cameron E., Driver S. P., 2007, MNRAS, 377, 523
Cameron E., Driver S. P., 2009, A&A, 493, 489
Capak P. et al., 2007, ApJ, 172, 99
Carollo C. M., 1999, ApJ, 523, 566
Carollo C. M., Stiavelli M., de Zeeuw P. T., Mack J., 1997, AJ, 114, 2366
Carollo C. M., Stiavelli M., de Zeeuw P., Seigar M., Dejonghe H., 2001, ApJ, 546, 216
Carollo C. M., Stiavelli M., Seigar M., de Zeeuw P. T., Dejonghe H., 2002, AJ, 123, 159
Carollo C. M., Scarlata C., Stiavelli M., Wyse R. F. G., Mayer L., 2007, ApJ, 658, 960
Coleman G. D., Wu C.-C., Weedman D. W., 1980, ApJS, 43, 393
Combes F., Debbasch F., Friedli D., Pfenniger D., 1990, A&A, 233, 82
Comerón S., Knapen J. H., Beckman J. E., Laurikainen E., Salo H., Martínez-Valpuesta I., Buta R. J., 2010, MNRAS, 402, 2462
Conselice C. J. et al., 2004, ApJ, 600, L139
Debattista V. P., Moore B., Quinn T., Katantaidis S., Maas R., Mayer L., Reed J., Stadel J., 2006, ApJ, 645, 209
de Vaucouleurs G., de Vaucouleurs A., Corwin H. G., Buta R. J., Jr, Paturel G., Fouqué P., 1991, Third Reference Catalogue of Bright Galaxies. Springer, New York
Elmegreen B. G., Elmegreen D. M., Chromey F. R., Hasselbacher D. A., Bissell B. A., 1996, AJ, 111, 1880
Elmegreen B. G., Elmegreen D. M., Hirst A. C., 2004, ApJ, 612, 191
Elmegreen D. M., Elmegreen B. G., Ravindranath S., Coe D. A., 2007, ApJ, 658, 763
Eskridge P. et al., 2000, AJ, 119, 536
Feldmann R. et al., 2006, MNRAS, 372, 565
Fontana A. et al., 2004, A&A, 424, 23
Foyle K., Rix H.-W., Zibetti S., 2009, preprint (arXiv:0911.2231)
Gadotti D. A., 2008, MNRAS, 384, 420
Graham A. W., Driver S. P., 2005, PASA, 22, 118
Heiderman A. et al., 2009, ApJ, 705, 1433
Hopkins P. F., Hernquist L., Cox T. J., Younger J. D., Besla G., 2009, ApJ, 688, 757
Ilbert O. et al., 2009, ApJ, 690, 1236
Jogee S. et al., 2004, ApJ, 615, L105
Kampczyk P. et al., 2007, ApJS, 172, 329
Kauffmann G. et al., 2003, MNRAS, 341, 33
Kinney A. L., Calzetti D., Bohlin R. C., McQuade K., Storchi-Bergmann T., Schmitt H. R., 1996, ApJ, 467, 38
Knapen J. H., Beckman J. E., Heller C. H., Shlosman I., de Jong R. S., 1995, ApJ, 454, 623
Knobel C. et al., 2009, ApJ, 697, 1842
Koekemoer A. M. et al., 2007, ApJS, 172, 196
Kormendy J., Kennicutt R. C., Jr, 2004, ARA&A, 42, 603
Kovac K. et al., 2010, ApJ, 718, 86
Laine S., Shlosman I., Knapen J. H., Peletier R. F., 2002, ApJ, 567, 97
Laurikainen E., Salo H., Buta R., Knapen J. H., 2007, MNRAS, 381, 401
Leauthaud A. et al., 2007, ApJS, 172, 219
LeFloc'h E. et al., 2009, ApJ, 703, 222
Lilly S. J. et al., 1998, ApJ, 500, 75
Lilly S. J. et al., 2007, ApJS, 172, 70
Lilly S. J. et al., 2009, ApJS, 184, 218
Lynden-Bell D., Kalnajs A. J., 1972, MNRAS, 157, 1
Marchesini D., van Dokkum P. G., Förster Schreiber N. M., Franx M., Labbé I., Wuyts S., 2009, ApJ, 701, 1765
Marinova I. et al., 2009, ApJ, 698, 1639
Méndez-Abreu J., Sánchez-Janssen R., Aguerri J. A. L., 2010, ApJ, 711, L61
Menéndez-Delmestre K., Sheth K., Schinnerer E., Jarrett T. H., Scoville N. Z., 2007, MNRAS, 657, 790
Nair P. B., Abraham R. G., 2010, ApJS, 186, 427
Oesch P. A. et al., 2010, ApJ, 714, L47
Pannella M. et al., 2009, ApJ, 701, 787
Pozzetti L. et al., 2007, A&A, 474, 443
Regan M. W., Elmegreen D. M., 1997, AJ, 114, 965

Rieke G. H., Alonso-Herrero A., Weiner B. J., Pérez-González B. M., Donley
    J. L., Marcillac D., 2009, ApJ, 692, 556

Robotham A., Phillipps S., de Propris R., 2010, MNRAS, 403, 1812

Sanders D. B. et al., 2007, ApJ, 172, 86

Sargent M. T. et al., 2007, ApJS, 172, 434

Sargent M. T. et al., 2010, ApJ, 714, L113

Scarlata C. et al., 2007, ApJS, 172, 406

Scoville N. Z. et al., 2007, ApJS, 172, 38

Sheth K., Regan M. W., Vogel S. N., Teuben P. J., 2000, ApJ, 532, 221

Sheth K., Vogel S. N., Regan M. W., Thornley M. D., Teuben P. J., 2005,
    ApJ, 632, 217

Sheth K. et al., 2008, ApJ, 675, 1141

Tasca L. A. M. et al., 2009, A&A, 503, 379

Trenti M., Stiavelli M., 2008, ApJ, 676, 767

Weinzirl T., Jogee S., Khochfar S., Burkert A., Kormendy J., 2009, ApJ,
    696, 411

Ziegler B. L. et al., 2002, ApJ, 564, 69

APPENDIX A: LOW-REDSHIFT COMPARISON SAMPLE

To provide a local Universe benchmark for comparison against the high-redshift bar fractions quantified here in the COSMOS data set we have constructed a complementary sample of low-redshift discs drawn from the SDSS.[2] From the visually classified SDSS galaxy catalogue presented by Nair & Abraham (2010) we have selected a subsample of 651 disc galaxies (S0− to Sd, $-3 \leq$ visual class ≤ 7) at $0.02 < z < 0.04$ with $M > 10^{10.5}$ M$_{\odot}$, axial ratio >0.7 (i.e. disc inclination $\lesssim 45°$), and $R_{\mathrm{e}} > 2.2$ kpc. At these redshifts the physical resolution scale (0.6–1.1 kpc/FWHM) and rest-frame wavelength coverage ($\sim$4000–7000 Å) of the ground-based SDSS *g*- and *r*-band imaging are roughly comparable to those of galaxies in our primary sample at $0.2 < z < 0.6$ in the space-based COSMOS *I*-band imaging ($\sim$4300–7000 Å and 0.4–0.8 kpc/FWHM).

To ensure consistency with our selection of barred galaxies in COSMOS we have applied an identical ellipse-fitting bar detection procedure to the SDSS comparison sample. For this purpose we downloaded the *u*-, *g*-, *r*-, *i*- and *z*-band images of all 651 disc galaxies in our local Universe sample from the SDSS imaging server (http://das.sdss.org/imaging/). Following the process described in Section 3.1, we recovered elliptical isophote profiles for each galaxy in the *g* and *r* bands using ellipse, and identified (strong) barred galaxy candidates as those objects with maximum ellipticity $e \geq 0.4$ and a subsequent drop of $\Delta e \geq 0.1$. Visual inspection of the *u*-, *g*-, *r*-, *i*- and *z*-band images of the barred galaxy candidates was then used to construct master catalogues of confident *g*- and *r*-band bar detections. During the visual inspection process six galaxies with axial ratio >0.7 were noted to be bulge-dominated S0s with near edge-on (rather than face-on) discs and were thus excluded in the subsequent analysis.

From the 588 intermediate-mass ($10^{10.5} < M < 10^{11}$ M$_{\odot}$) disc galaxies in our local Universe sample we identify 214 barred systems (a bar fraction of 36 per cent) in the *g* band and 240 barred systems (41 per cent) in the *r* band. From the 57 high-mass ($M > 10^{11}$ M$_{\odot}$) disc galaxies we identify only nine barred systems
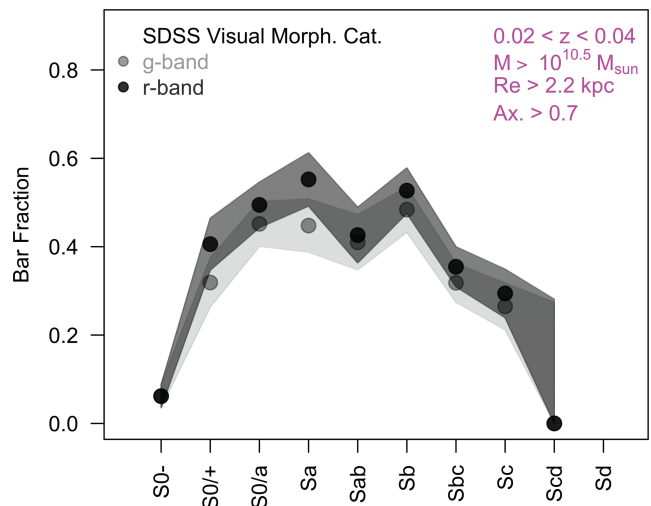
[2] Whilst there already exists a valuable data base of SDSS systems artificially redshifted to $0.7 < z < 1.2$ and matched to the PSF and S/N of the COSMOS ACS *I*-band imaging provided by Kampczyk et al. (2007), the effective resolution of these artificially redshifted galaxies is much lower than that for the $0.2 < z < 0.6$ COSMOS disc sample employed in this study, and thus not suitable for the present analysis.

Figure A1. The bar fraction by visual morphological class for massive ($M > 10^{10.5}$ M$_{\odot}$) discs at axial ratio >0.7 and $R_{\mathrm{e}} > 2.2$ kpc in the local Universe ($0.02 < z < 0.04$). The visual morphological classifications are from the Nair & Abraham (2010) catalogue. The bar fractions recovered via application of the ellipse-fitting method (described in Section 3.1) to the SDSS *g*- and *r*-band images of each galaxy are compared here to demonstrate the minimal dependence of bar detection efficiency on (optical band) wavelength across all morphological types.

(16 per cent) in the *g* band and 10 barred systems (18 per cent) in the *r* band. The difference of $\sim$12 per cent between the bar fractions recovered here in the *g* and *r* bands is slightly higher than that of $\sim$5 per cent reported in the analysis of a high resolution ($D < 100$ Mpc) SDSS sample by Sheth et al. (2008). However, we note that the majority of bars missed by our *g*-band ellipse-fitting lie in compact galaxies with $2.2 < R_{\mathrm{e}} \lesssim 3$ kpc. Hence, we suspect that the larger PSF FWHM in the SDSS *g*-band images (FWHM $\sim$ 1.5 arcsec) relative to the *r* band (FWHM $\sim$ 1.4 arcsec) was the cause of the bar detection failures for these compact systems. At $R_{\mathrm{e}} > 3$ kpc the difference in recovered bar fractions between the *g*- and *r* bands in our sample is only 6 per cent. In Fig. A1 we contrast the dependence of bar fraction on disc morphological type (at $R_{\mathrm{e}} > 2.2$ kpc) recovered using our *g*- and *r*-band ellipse-fit catalogues in order to demonstrate the minimal dependence of bar detection efficiency on (optical band) wavelength across all morphological types.

In Table A1 we present the bar fractions in our local Universe comparison sample subdivided by mass, morphological type, SSFR and environmental density as performed for our high-redshift disc sample in Section 4. Specifically, we employ the Kauffmann et al. (2003) stellar masses to separate our SDSS sample into intermediate-mass systems at $10^{10.5} < M < 10^{11}$ M$_{\odot}$ and high-mass systems at $M > 10^{11}$ M$_{\odot}$. Early- and late-type discs are defined as those with visual morphological classes S0− to Sa and Sb to Sd, respectively. To define our low (high) SSFR and density populations we adopt the Brinchmann et al. (2004) SSFR estimates and Baldry et al. (2006) environmental densities (average of Σ_4 and Σ_5), and identify the lowest (highest) thirds of each distribution.

A comparison of these local Universe bar fractions against those recovered at high redshift in COSMOS is presented in Section 4. As described therein, the SDSS bar fractions by stellar mass and spectral/morphological type confirm the evolutionary trends observed for massive barred galaxies over the redshift interval $0.2 < z < 0.6$ in COSMOS.

Table A1. Bar fractions by mass, morphology, SSFR and environmental density in an SDSS local Universe comparison sample.

Bar catalogue	Stellar mass[a]	Morphological type	SSFR[a]	Environmental density[a]
r-band ellipse fit	Intermediate	Early-type: $f_{bar} = 0.40 \pm 0.03$	Low SSFR: $f_{bar} = 0.49 \pm 0.04$	High density: $f_{bar} = 0.48 \pm 0.04$
r-band ellipse fit	Intermediate	Late-type: $f_{bar} = 0.41 \pm 0.03$	High SSFR: $f_{bar} = 0.34 \pm 0.03$	Low density: $f_{bar} = 0.39 \pm 0.03$
r-band ellipse fit	High	Early-type: $f_{bar} = 0.13 \pm 0.06$	Low SSFR: $f_{bar} = 0.21 \pm 0.09$	High density: $f_{bar} = 0.21 \pm 0.09$
r-band ellipse fit	High	Late-type: $f_{bar} = 0.22 \pm 0.08$	High SSFR: $f_{bar} = 0.05 \pm 0.05$	Low density: $f_{bar} = 0.16 \pm 0.08$

[a]Here we define intermediate stellar mass as $10^{10.5} < M < 10^{11}\ M_{\odot}$ and high stellar mass as $M > 10^{11}\ M_{\odot}$, and we identify the low and high SSFR (or environmental density) populations as the lower and upper thirds of the SSFR (or environmental density) distribution in each mass and redshift bin. The SDSS disc sample examined is also restricted to systems with axial ratio >0.7 and $R_e > 2.2$ kpc as described in this appendix.

This paper has been typeset from a TEX/LATEX file prepared by the author.